Optics & Laser Technology 161 (2023) 109117

Contents lists available at ScienceDirect

Optics and Laser Technology

journal homepage: www.elsevier.com/locate/optlastec

Full length article

Formation and manipulation of 2D colloidal crystals driven by convective currents and electrostatic forces

J. Ramírez-Ramírez [a], J.A. Sarabia-Alonso [a,b], J. Vázquez-Lozano [a], H. Peregrina-Barreto [a], S. Mansurova [a], R. Ramos-García [a,*]

[a] Departamento de Óptica, Instituto Nacional de Astrofísica, Óptica y Electrónica, Luis Enrique Erro #1, Puebla C.P. 72840, Mexico
[b] División de Posgrado, Universidad Politécnica de Tulancingo, Tulancingo, Hidalgo C.P. 43629, Mexico

ARTICLE INFO

Keywords:
Optothermal effects
Optical trapping
Convective currents
Thermal gradient

ABSTRACT

Colloidal crystal plays a major role in novel optical devices such as waveguides, photonic crystals, and colloidal crystal lasers, among others. It has been known that colloidal crystals may self-assemble due to optical, electric, or chemical potentials, and light-induced thermal effects, such as thermophoresis and convective currents. In this work, the formation and manipulation of a self-limiting assembly of monolayer colloidal crystals using a 20 nm absorbing thin film of titanium and a CW-laser emitting at 1070 nm is reported. The colloidal particles, dragged by thermally induced convective currents, self-assembling over the titanium thin film around the laser focal spot. The self-assembled monolayer colloidal crystal tends to form a circular shape. Using numerical simulation, we obtained a potential well associated with the convective currents that spatially govern the radial extension of the monolayer colloidal crystal. We also show, that by changing the pH of the solution i.e., by tuning the electrostatic interaction, the monolayer colloidal crystal can be formed or destroyed. In addition, it was possible to create a larger monolayer colloidal structure covering an area of 600 μm^2 using an array of six laser spots.

1. Introduction

Colloidal crystals [1,2] play a crucial role in the design of novel optical devices such as waveguides [3], photonic crystals [4], and colloidal crystal lasers [5], among others. These applications have been addressed through techniques like nanoimprinting [6], photolithography [7], and self-assembly [8,9]. The latter has the advantage of not requiring an external mechanism or device for overcoming the several dynamic processes behind the assembly of colloidal particles. Among the self-assembly methods those driven by optothermal effects, have emerged as a promising strategy by their universal applicability in several colloidal systems and low technical requirements. Several authors have investigated monolayer colloidal crystal formation using thermal effects, for example, Braun *et al.* [10,11] reported the accumulation of polystyrene particles into colloidal crystals driven by convective currents and thermophoresis. Dholakia *et al.* [12] demonstrated the self-assembly of 5 μm silica particles into an extended hexagonal close-packed array using convective currents excited by the thermoplasmonic effect. In a similar configuration, Zhiwen Kang *et al.* [13] attributed to thermophoretic and convective currents, while Di Leonardo [14] using a dielectric absorbing substrate attributed to a Marangoni-like effect. All these reports share similar experimental conditions: a light-absorbing (typically gold) substrate that is heated up by light absorption from a laser beam giving rise to thermally induced effects like thermophoresis, convective currents, and Marangoni-like effects. Nevertheless, no analysis of the colloidal crystal configuration, stability, and its spatial extension has been reported to our knowledge.

In this work, we present the generation and 2D manipulation of monolayer colloidal crystals by self-assembly of silica particles and explore the particle interactions, i.e., electrostatic stabilization. Moreover, using numerical simulation, we obtain a potential well associated with the convective currents that radially determines the spatial extension of the monolayer colloidal crystal. By changing the pH of the solution, we modulated the inter-particle interaction forces, i.e., van der Waals and double electric layer. The tunning of the inter-particles forces allows the well-order of the colloidal particles and controls the stability of the colloidal crystal. Finally, we show the generation of a much larger monolayer colloidal structure of 600 μm^2 (30 μm × 20 μm) by employing an array of six laser spots.

* Corresponding author.
E-mail address: rgarcia@inaoep.mx (R. Ramos-García).

https://doi.org/10.1016/j.optlastec.2023.109117
Received 2 August 2022; Received in revised form 21 November 2022; Accepted 3 January 2023

2. Experimental setup

To perform the experiments, we prepared a colloidal solution of silica beads (SiO_2, 1 μm diameter, concentration of 10 % solids weight/volume, ~ 1.01x10^{11} particles/ml, Polysciences Inc.) dispersed in distilled water and placed between sealed glass coverslips keeping 20 μm of separation between coverslips. The solution for trapping was prepared with 20 μL of the colloidal solution of silica beads and 980 μL of distilled water, so the final colloidal solutioń s concentration was 0.2 %. Using a micropipette, the pH of the colloidal solution was adjusted by adding 0.5 μL of either an alkaline substance (NaOH, 7 > pH) or an acidic one (HCl, 7 < pH), until the desired pH level was achieved based on the measurements performed with a pH/T meter (Mi150 by Milwaukee Instruments). On the lower coverslip, a 20 nm titanium (Ti) film was previously deposited by sputtering. The experiment was carried out using a commercial optical tweezers system (OTS, E3500 by Elliot Scientific) coupled to an inverted microscope with an oil immersion objective (100x, NA = 1.45), as depicted in Fig. 1. A CW fiber laser beam (emitting at 1,070 nm and 1 W maximum power), was employed to irradiate the Ti thin film and its optical power is fine-tunned with a variable attenuator consisting of a $\lambda/2$ waveplate and a polarized cube beam splitter. The OTS is equipped with an acousto-optic deflector (AOD) that allows the generation of multiple spots at the trapping plane. Even though any metal or absorbing dielectric works fine, however, Ti is preferred for its toughness, corrosion resistance, and its easy adhesion to glass, in addition, possesses a high absorption coefficient. Furthermore, no plasmons needed to be excited as opposed to gold, simplifying the experimental setup.

3. Numerical simulation

Light absorption at the Ti thin-film (α_{Ti} ~ 5.1 x10^7 m^{-1} [15]) generates a temperature gradient (∇T) that heats the distilled water up according to the heat equation, given by [16,17]:

$$\rho c_p \boldsymbol{u} \bullet \nabla \boldsymbol{T} = \nabla \bullet (\kappa \nabla \boldsymbol{T}) + Q \tag{1}$$

where ρ is the distilled water density, c_P is its heat capacity, $\boldsymbol{u}$ is the velocity of the fluid field, κ is the thermal conductivity; $Q = I_0\,\alpha$ is the heat source per volume unit, where α is the absorption coefficient and I_0 is the optical source intensity. Since the light absorption coefficient of Ti is approximately six orders of magnitude greater than the distilled water one, the Ti thin film plays as the only heat source. As the laser is on, convective currents with a toroidal shape close to the laser beam spot and thermophoretic forces take place. To determine the magnitude of these convective currents, we solved the Navier-Stokes equations coupled with the heat equations in COMSOL Multiphysics [16,17]:

$$\rho(\boldsymbol{u} \bullet \nabla)\boldsymbol{u} = \nabla \bullet \{ -p\boldsymbol{I} + \mu[\nabla \boldsymbol{u} + (\nabla \boldsymbol{u})^T] \} + \boldsymbol{F}_b \tag{2}$$

$$\rho \nabla \bullet \boldsymbol{u} = 0 \tag{3}$$

Here we assume that a Gaussian beam is incident on the Ti thin-film, p is the pressure of the fluid, μ is the dynamic viscosity of the fluid, and $\boldsymbol{I}$ is the 2nd order identity tensor. $\boldsymbol{F}_b = \boldsymbol{g}(\rho - \rho_0)$ where ρ and ρ_0 are the water's densities after the laser has been turned on and at room temperature, respectively. The intensity distribution of the incident Gaussian beam is given by:

$$I_{Ti}(r,z) = T_{net}\frac{2P}{\pi\omega^2(z)}\exp[-\alpha_{Ti}(z + l_{water})]\exp\left(-\frac{2r^2}{\omega^2(z)}\right) \tag{4}$$

where $T_{net} \approx 0.27$ is the net transmission that involves all Fresnel losses at the interfaces of the glass cell. P = 3.1 mW is the laser beam power and $\omega(z)$ is the laser beam radius defined as:

$$\omega(z)^2 = \omega_0^2\left[1 + \frac{z^2}{z_R^2}\right] \tag{5}$$

where $z_R = \frac{\pi\omega_0^2}{\lambda}$ is Rayleigh distance and ω_0 is the beam waist. The focal plane is placed 1 μm above the Ti thin film. The light is strongly absorbed on the Ti thin film. Photoexcited electrons relax non-radiatively increasing the temperature of the film and the surrounding liquid, generating a temperature gradient around the beam position, and setting up in motion convective currents within the cell, as indicated by the white arrows in Fig. 2.

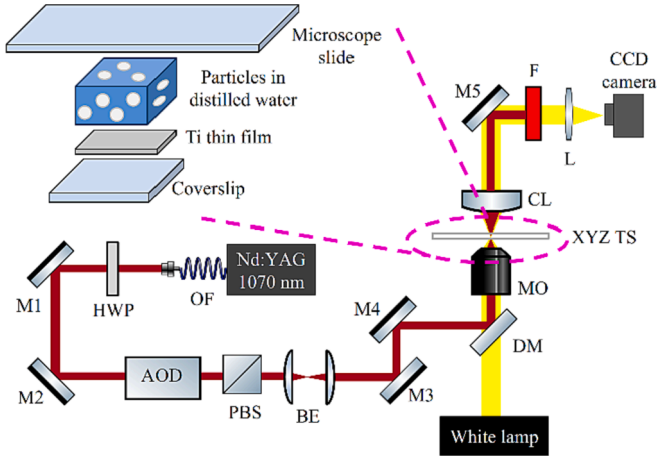

Fig. 1. Sketch of the commercial Optical Tweezers System E3500 Elliot Scientific. The power of the laser beam (CW laser with optical fiber output OF) is fine-tuned with a half-wave plate HWP and a polarizing beam splitter PBS, then the laser beam is expanded by a beam expander BE and redirected with a couple of mirrors and a dichroic mirror (DM) to a 100x oil immersion microscope objective (MO) with NA = 1.45. CL is a condenser lens, XYZ TS is the translation stage for providing 3D control motion of the sample, and F is a filter that blocks the reflected light to avoid saturation on the CCD camera. The same MO is employed to image the silica microparticles on the CCD camera. The illumination is provided by a white lamp source. The acousto-optic deflector AOD allows the generation of multiple spots at the trapping plane.

4. Results and discussions

When the laser was turned on, the dispersed silica microparticles were dragged from remote regions (~15–20 μm) towards the laser beam spot. Fig. 3(a) shows the tracking of only 6 particles as they converged

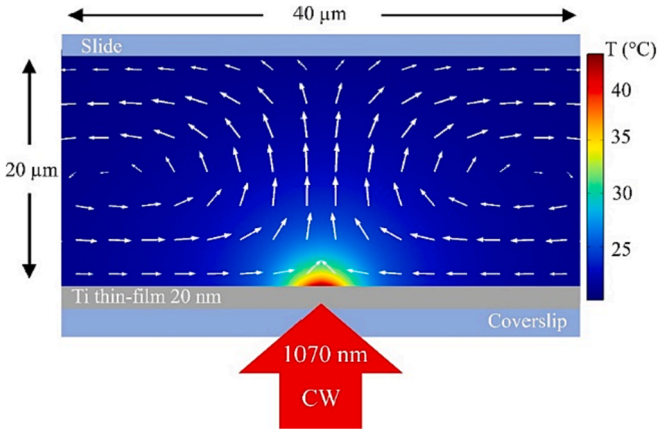

Fig. 2. Schematic representation of the formation of the convective currents. Silica particles are dragged toward the hot spot by the convective currents, represented by the white arrows. The length of the arrows is proportional to the magnitude of the convective currents. The maximum temperature (42° C) reached occurs at z = 0.5 μm. For the sake of illustration, only 40 μm (out of 20 mm) of the length of the cell is shown. Figure not in scale.

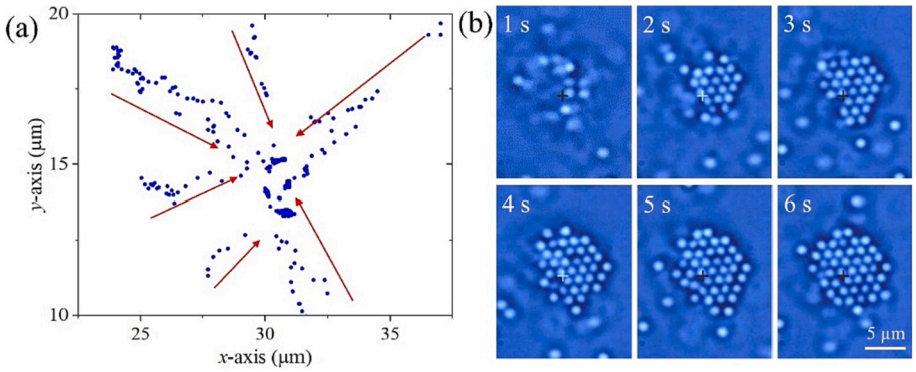

Fig. 3. (a) Trajectory of 6 particles attracted towards the laser beam (hot zone). The blue dots represent the centroids of the particles, and the red arrows show the direction of the particlés movement. (b) Snapshot of the dynamic formation of a monolayer colloidal crystal. See **Visualization 1.** (For interpretation of the references to colour in this figure legend, the reader is referred to the web version of this article).

and self-assembled in an open boundary monolayer colloidal crystal. The particles tracking was carried out by a homemade MATLAB code. The focal position was set at the Ti thin film and since the trapped microparticles remain in focus, one can safely assume that they move along the substrate. The beam power was sufficiently low such that the scattering force and the upwards drag force could not compensate for gravity and the attractive van der Waals forces between the particles and the substrate. On the other hand, beam powers above 3.5 mW, activates thermophoresis resulting in particles being expelled from the hot region, creating a ring of particles where the thermophoretic and drag forces compensate as previously reported [16]. Even higher power leads to bubble formation and cavitation [17,18]. Thicker Ti films decreases the threshold values for the several regimes described above. All results presented here will be in the convective current-dominated regimen.

Fig. 3(b) shows snapshots of the dynamic formation of the monolayer colloidal crystal using 3.1 mW of laser power. Notice that the crystal is formed within 2 s and is fully formed in 6 s. It was noticed that the colloidal crystal reached a maximum diameter of around 10 μm, as it is shown in **Visualization 1.** Although the laser was on for up to 30 min, the colloidal crystal did not increase its size, even if the particle concentration was increased. In fact, one can observe that some microparticles approached the crystal but did not stick to it.

To understand the limited size of the colloidal crystal, the velocity of the convective current that drag the particles is analyzed from the numerical simulations. Fig. 4(a) shows the transversal drag force gradient ($\boldsymbol{F}_d = 6\pi\mu R\boldsymbol{u}$), associated with the convective current's velocity profile ($\boldsymbol{u}$) perpendicular (we chose 0.5 μm above the substrate because of the particles radius) to the beam propagation. Note that for $r > 40$ μm the drag force is negligible, then reaches its peak at ~ 5 μm and finally finds a minimum around $r = 0$ (See Fig. 4(a)). Since the velocity profile is spatially varying, so does the drag force. Note that the force is zero at $r = 0$, so if the particle moves to either the left or right, there will be a restoring force that attracts the particle back to its original position, i.e., we can associate a potential well to the drag gradient force in analogy to the optical gradient force [17]. Fig. 4(b) shows the potential well calculated from the linear region of the drag gradient force exhibiting a parabolic shape. From the analysis of Fig. 4(a-b), we can foretell that the particles will tend to self-assemble around the minimum of the potential well that extends radially approximately between -5 μm $< r < 5$ μm, i.e., 10 μm of diameter, in agreement with the experiment. Therefore, the spatial extension of the monolayer colloidal crystal is determined by the spatial extension of the potential well.

Once the colloidal crystal was formed, 2D manipulation of the crystal was accomplished by moving either the translation stage or the laser spot, as shown in **Visualization 1**. If the laser is turned off, the convective currents disappear i.e., the trapping potential disappears and the electrostatic repulsion force and Brownian motion of the microparticles rapidly destroy the monolayer colloidal crystal. It was reported theoretically, that a monodisperse colloidal system of N particles under the influence of a parabolic potential well, such as the one shown in Fig. 4(b), can assemble in different stable configurations such as square, triangular, or a mix of both [19]. The configuration depends on the nature of the particles' interaction, which is a combination of a hard-core interaction within a distance of $2R$, with R being the hard-core particle radius, and a softcore repulsion within a distance $r > 2R$. Using a homemade MATLAB code, the angle between the centroid of a particle and the centroid of its neighbors[19] (distance between neighboring centroid < 2.6 particle radius) was measured and it determined that the crystal always assumed a triangular configuration (see Fig. 5). The crystals show a stable configuration even while is being

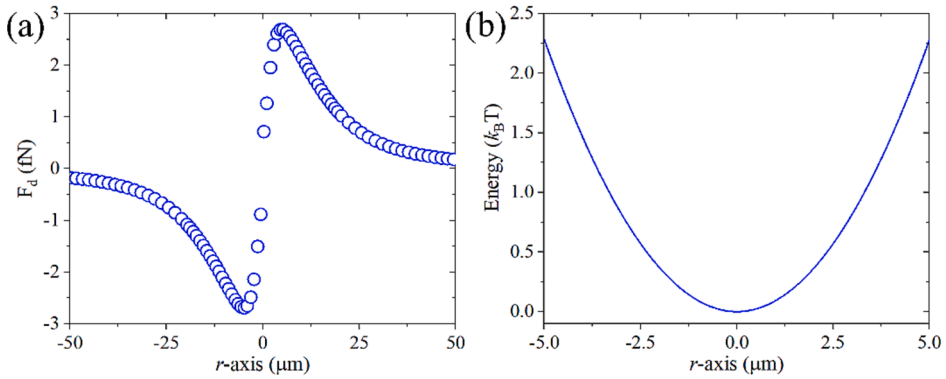

Fig. 4. (a) Transversal drag force gradient associated with the transversal convective currents profile at 0.5 μm above the Ti thin-film, extracted from numerical simulations performed with COMSOL Multiphysics. (b) A potential well is obtained from the linear region of the transversal drag force shown in (a).

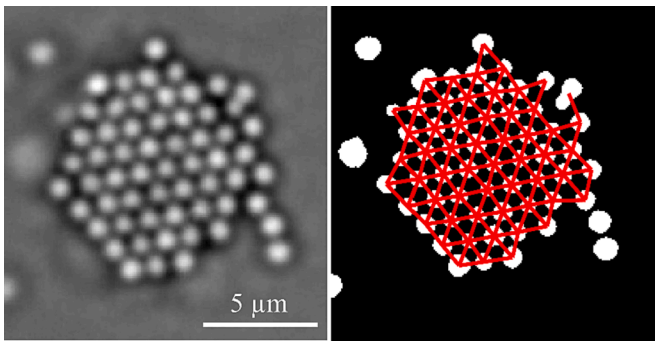

Fig. 5. (a) Silica microparticles self-assembled in a monolayer colloidal crystal employing a power of 3.1 mW, extracted from **Visualization 1**; (b) The triangular configuration of the monolayer is always obtained.

manipulated except for particles around its border.

When the colloidal crystal is formed, the mean displacement of the constituent microparticles decreases due to the inter-particle interaction. This was assessed by calculating the diffusion constant from the median square displacement (*MSD*). According to the literature [20], $MSD = 2Dt$, where t is time and D is the particlés diffusion constant. Fig. 6 shows the *MSD* of a microparticle around the center of the crystal (Fig. 5) when the crystal is fully formed and one second just after the laser is turned off. We notice that the diffusion constant increases from 0.2 $\mu m^2/s$ to 0.35 $\mu m^2/s$, while the diffusion constant of quasi-isolated particles is $\sim$ 0.8 $\mu m^2/s$. This indicated that the Brownian motion and the presence of a repulsive force (probably due to surface charge on the microparticle) destroy the crystal.

In the absence of the hydrodynamic dragging forces, the stability of the colloidal crystal is determined by the balance between short-range attractive van der Waals forces and long-range repulsive electrostatic forces. Too high repulsive potential barrier may prevent the particles from getting closer to forming an ordered structure. In the opposite case of too low repulsive barrier (or no barrier at all), an attractive force may lead to particle agglomeration and sedimentation. The relative magnitudes of these forces can be tuned by changing the surface charge of the

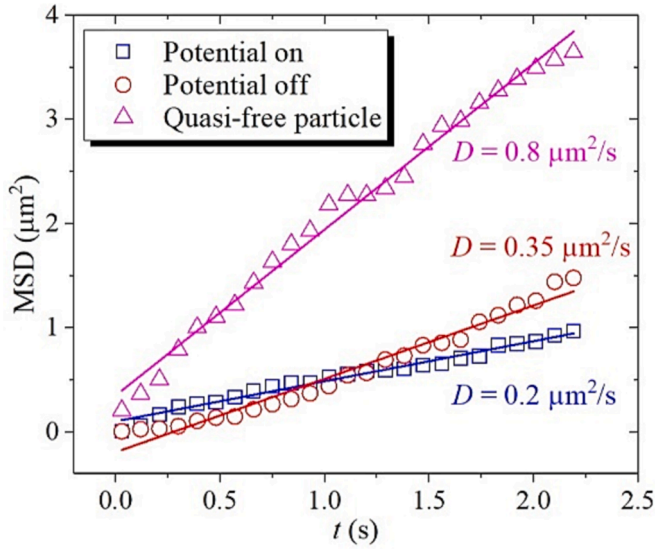

Fig. 6. Particle's diffusion constant of silica particles in distilled water. The red circles represent the tracking of a particle near the center of the crystal, the blue squares the same particle almost immediately after the laser has been turned off and the magenta triangles represent a quasi-isolated particle. Solid lines are linear fits to the experimental data. (For interpretation of the references to colour in this figure legend, the reader is referred to the web version of this article).

particles and/or by screening the potential caused by these surface charges. Next, we will consider how this tuning can be achieved by changing the acidity of the solution.

The amount of surface charges is controlled by the interplay of the microparticle's surface chemistry and that of the surrounding solution. It is well known, that the SiO_2 surface reacts with water to form a layer of silanol (SiOH) groups. These groups can be either positively or negatively charged depending on the acidity of the solution. It is mainly assumed that silanol groups on the silica surface are protonated for pH < 2 and fully deprotonated for pH > 4 [21–23]. Thus, it is reasonable to assume that silica particles are positively charged in water for a pH value < 2 and negatively charged at a pH value > 4 [24]. For pH values in between there are mostly Si–OH groups on the surface, hence, the surface is globally neutral (this is the so-called point of zero charge) and the repulsive electrostatic forces between the particles are negligible. In this regime, the system is most unstable, since short-range attractive van der Waals forces become dominating, which leads to colloid particle aggregation. When the pH value increases (pH > 4), the surface negative charge increases, and long-range electrostatic repulsions become more and more important.

Note, that pH modification also affects charges on the titanium surface which is covered by a thin native oxide layer (mainly amorphous TiO_2) due to the passivation by oxygen from the air, which is about 3–7 nm thick [25]. Like SiO_2, this surface is highly hydroxylated and when it gets in contact with water, both positive and negative charges are formed. However, in contrast to SiO_2, the point of zero charges for TiO_2 lies between 5 $<$ pH $<$ 6.6 [26].

The excess of charge on the particle surface in aqueous solutions gives rise to an electrical double layer as counter ions in the adjacent solution rearrange to screen the charge. The structure of the electrical double layer takes the form of a charged surface layer and an outer Stern layer, consisting of a film of counter ions around the microparticle surface. Outside the Stern layer, there is a diffuse layer of positive and negative ions, screening the net surface charge over a characteristic Debye length L_D [27]. The Debye length determines the distance from the particles surface where the electrostatic potential, is reduced to $1/e$ of its initial value. The Debye length depends on the counter ions concentration (in bulk) c as the inverse square root, $L_D \propto (c)^{-1/2}$. At a small concentration of ions surrounding the microparticle, (i.e., low ionic strength of the solution) the Debye screening length is large and the electrostatic repulsive forces are dominant, preventing particle aggregation [28]. On the opposite case of high counter ions concentration (i.e., high ionic strength of the solution), the Debye length is small, hence electrostatic repulsion is effectively screened. In this situation, particles can overcome the repulsive potential barrier and fall in the van der Waals attractive potential which leads to particles agglomeration. Usually, the ionic strength of the solution is modified by adding ionic salts (e.g., NaCl), however, changing the acidity also affects the concentration of counter ions or charged species in the colloidal suspensions [29,30]. When the pH is very low (i.e., the solution is strongly acidic) or very high (i.e., the solution is strongly basic), the ionic strength of the solution increases [31,32]. To investigate the pH influence on the formation of circular-shape monolayer colloidal crystals and their manipulation, we prepared colloidal suspensions with different pH values ranging from 1 to 11.

At low pH values (pH = 1.5, not shown in Fig. 7) fast sedimentation of the particles over the Ti-thin film was observed such that no manipulation of the microparticles was possible. In this pH range both, particles and Ti substrate are positively charged. However, sedimentation and consequent adhesion to the Ti substrate can be explained by the fact that a very acidic solution possesses high ionic strength. Therefore, the Debye length is reduced so much that the van der Waals force governs both the inter-particle interactions and the Ti-microparticles interactions.

At pH = 3, some silica particles still adhere to the Ti thin film,

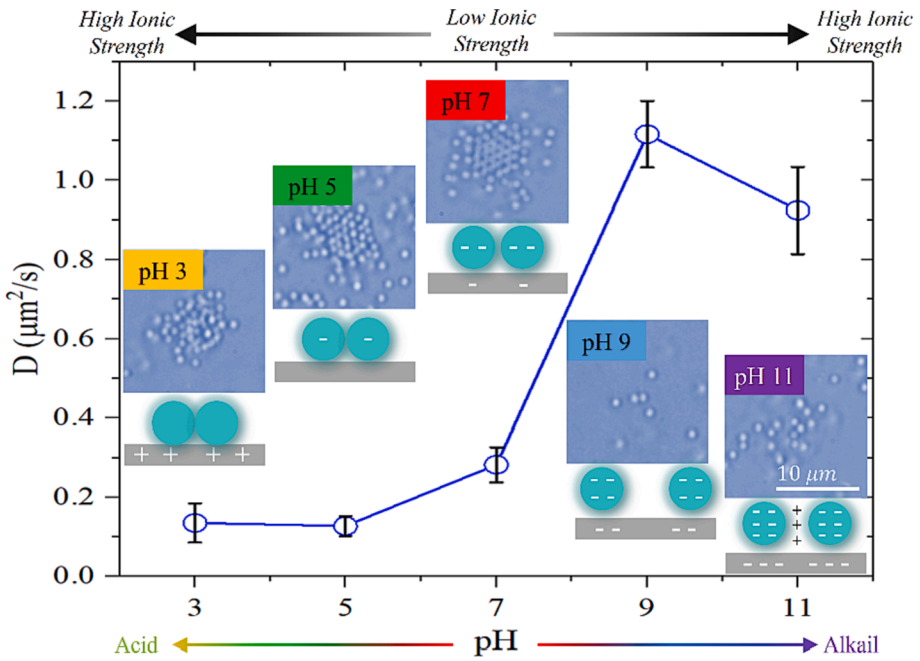

Fig. 7. Diffusion coefficients as a function of pH concentrations extracted from **Visualization 2**. For pH ranging from 3 to 7, self-assembly and manipulation were possible whereas, for 9 and 11, only manipulation was observed. See **Visualization 2**.

whereas others can be dragged by the convective currents, i.e., hydrodynamic drag forces. These particles exhibit a strong tendency to aggregate without a well-defined structure. However, agglomerated particles may still be manipulated. Particles' agglomeration and ease of the manipulation in this acidity range occur due to the action of dragging force and the absence of repulsion since most of the particles are globally neutral (few positively charged particles stick to the substrate). However, in the absence of the repulsion forces, no assembly of ordered monolayer is possible. On the other hand, being neutral, the particles are laying upon the positively charged substrate and the dragging force is less efficient, both due to the friction and reduction of the dragging force in the proximity of the substrate/water interface.

At pH = 5, more silica particles are gathered by convective currents until they aggregate forming a structure with a small degree of order of particles in the center and disordered/non-perfectly formed areas at the edges, as is shown in **Visualization 2**. In this pH interval microparticles possess a small negative charge, so the interplay of the repulsive forces and dragging forces (both long-ranged) initializes the formation of ordered arrays. On the other hand, the Ti substrate is mostly neutral, and the dragging force is less efficient again.

The case of neutral solution at pH = 7 seems to be the optimal condition for the formation of a stable, highly ordered monolayer of the colloidal crystal. Increased negative surface charge together with large Debye length (low ionic strength) provides effective electrostatic repulsion, preventing particle's aggregation. On the other hand, the dragging force potential well maintains the particles trapped preventing the spreading of particles due to thermal motion and electrostatic repulsion. It is worth to mention, that the obtained monolayer can be easily manipulated and displaced as a whole without perturbing the structure.

At pH = 9, the particles do not come into contact indicating that due to the increased negative surface charges, electrostatic repulsion forces are now dominant relative to the joint action of van der Waals attraction forces and hydrodynamic dragging forces. Finally, at higher pH values ($\geq$ 9) Fig. 7, the silica particles seem to be able to gather again (though in a disordered manner). This might occur due to the increased ionic strength of the solution in the high pH end, thus reducing the Debye screening length, and increased repulsion is now partially compensated by more effective screening.

Both surface charge and the presence of extra ions in the solution may affect the diffusion of the colloidal particles [28]. By tracking the displacement of the particles, the diffusion constant, *D*, of the colloidal particles immersed in the aqueous solution at different pH values was measured. One can see that the particle's diffusion coefficient is almost unchanged at low pH values indicating that they are effectively confined in a potential well created by convective currents. However, at pH 9 the diffusion coefficient increases sharply, and its value is close to that of the free (non-confined) particle, indicating that electrostatic potential energy is higher than the depth of the potential well created by the dragging force gradient. For pH > 9 higher ionic strength causes a reduction of the Debye length and therefore a more effective shielding of the original charge of the particle leading to a decrease in the diffusion coefficient.

Finally, it was possible to build a much larger monolayer of colloidal crystal with an array of trapping spots. For this experiment, the concentration of the working colloidal solution was increased 3 times. To achieve this, one single spot assembled a $\sim$ 10 μm diameter monolayer colloidal crystal until it stopped growing. Once this was achieved, another beam was placed at a distance 2 times the radii of the previous monolayer colloidal crystal. This again created a crystal that was pieced together with the previous one. This can be performed several times depending on the desired size. In this experiment, the total number of spots used was 6, forming a monolayer colloidal crystal with dimensions $\sim$ 30 μm $\times$ 20 μm, as shown in Fig. 8. Defects and configurations other than the triangular structure can be observed along the boundaries of the individual colloidal crystals, however, by decreasing the spacing between spots it is possible to reduce or even eliminate them.

5. Conclusions

In summary, we have presented a simple, yet effective technique to create and manipulate a 2D circular-shape monolayer colloidal crystals of silica particles under convective currents induced by light absorption from a CW at low optical power. Using numerical simulation, we obtain a potential well associated with the convective currents that determines the radial spatial extension of the monolayer colloidal crystal. By

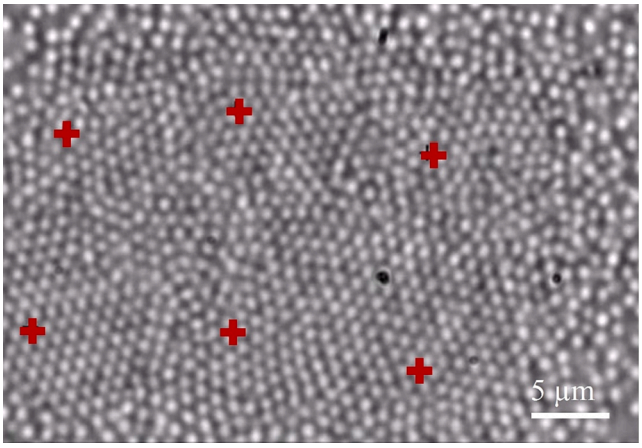

Fig. 8. Assembly of a larger crystal by the inclusion of 6 laser beams (indicated by the red cross). (For interpretation of the references to colour in this figure legend, the reader is referred to the web version of this article).

changing the pH of the solution, we modulated the inter-particles and particle–substrate interaction forces (i.e., van der Waals and electrostatic forces). The tunning of the inter-particles forces allows us to find the conditions with the enhanced stability of the colloidal crystal leading to the creation of the well-ordered colloidal particle monolayer which can be easily manipulated. Finally, we show the generation of a much larger well-formed monolayer colloidal crystal by employing an array of six laser spots creating a monolayer colloidal crystal of 600 μm^2 (30 μm × 20 μm). This technique neither requires chemical particle modification nor UV curing nor a long process time to create the colloidal crystals, besides it may allow real-time dislocation corrections. Therefore, our proposal means both non-contact and non-invasive approaches to address the problem of the colloidal particles ordered 2D arrays assembling.

Funding

This work was financially supported by the Mexican Council of Science and Technology (CONACyT) (OISE:PIRE-SOMBRERO)/(CONACyT 251992, grant 261148).

7. Data availability statement

Derived data supporting the findings of this study are available from the corresponding author [MCA] on request.

8. Data availability

The data that support the findings of this study are available within the supplementary material and from the corresponding authors upon reasonable request.

CRediT authorship contribution statement

J. Ramírez-Ramírez: Conceptualization, Data curation, Formal analysis, Investigation, Resources, Software, Validation, Visualization, Writing – original draft. **J.A. Sarabia-Alonso:** Conceptualization, Data curation, Formal analysis, Investigation, Resources, Software, Validation, Visualization, Writing – original draft, Writing – review & editing. **J. Vázquez-Lozano:** Conceptualization, Formal analysis, Resources, Validation, Writing – original draft, Writing – review & editing. **H. Peregrina-Barreto:** Data curation, Software. **S. Mansurova:** Conceptualization, Formal analysis, Writing – original draft, Writing – review & editing. **R. Ramos-García:** Conceptualization, Formal analysis, Funding acquisition, Project administration, Resources, Supervision, Visualization, Writing – original draft, Writing – review & editing.

Declaration of Competing Interest

The authors declare that they have no known competing financial interests or personal relationships that could have appeared to influence the work reported in this paper.

Data availability

Data will be made available on request.

Appendix A. Supplementary material

Supplementary data to this article can be found online at https://doi.org/10.1016/j.optlastec.2023.109117.

References

[1] P. Pawel, Colloidal crystals, Contemp. Phys. 24 (1983) 25.
[2] B. Li, D. Zhou, Y. Han, Assembly and phase transitions of colloidal crystals, Nat. Rev. Mater. 1 (2016) 1.
[3] S.A. Rinne, F. García-Santamaría, P.V. Braun, Embedded cavities and waveguides in three-dimensional silicon photonic crystals, Nat. Photonics 2 (2008) 52.
[4] J. Ge, Y. Hu, Y. Yin, Highly tunable superparamagnetic colloidal photonic crystals, Angew. Chemie - Int. Ed. 46 (2007) 7428.
[5] A. Mikosch, S. Ciftci, A.J. Kuehne, Colloidal crystal lasers from monodisperse conjugated polymer particles via bottom-up Coassembly in a sol-gel matrix, ACS Nano 10 (2016) 10195.
[6] S.Y. Chou, P.R. Krauss, P.J. Renstrom, Nanoimprint lithography, J. Vacuum Sci. Technol. B: Microelectr. Nanometer Struct. Process. Measure. Phenom. 14 (1996) 4129.
[7] Z. Zhang, C. Geng, Z. Hao, T. Wei, Q. Yan, Recent advancement on micro-/nano-spherical lens photolithography based on monolayer colloidal crystals, Adv. Colloid Interface Sci. 228 (2016) 105.
[8] S.H. Kim, S.Y. Lee, S.M. Yang, G.R. Yi, Self-assembled colloidal structures for photonics, NPG Asia Mater. 3 (2011) 25.
[9] K. Barkan, M. Engel, R. Lifshitz, Controlled self-assembly of periodic and aperiodic cluster crystals, Phys. Rev. Lett. 113 (2014) 1.
[10] S. Duhr, D. Braun, Two-dimensional colloidal crystals formed by thermophoresis and convection, Appl. Phys. Lett. 86 (2005) 1.
[11] M. Jerabek-Willemsen, C.J. Wienken, D. Braun, P. Baaske, S. Duhr, Molecular interaction studies using microscale thermophoresis, Assay Drug Dev. Technol. 9 (2011) 342.
[12] V. Garcés-Chávez, R. Quidant, P.J. Reece, G. Badenes, L. Torner, K. Dholakia, Extended organization of colloidal microparticles by surface plasmon polariton excitation, Phys. Rev. B - Condens. Matter Mater. Phys. 73 (2006) 1.
[13] Z. Kang, J. Chen, S.Y. Wu, H.P. Ho, Plasmonic absorption activated trapping and assembling of colloidal crystals with non-resonant continuous gold films, RSC Adv. 5 (2015), 105409.
[14] R. Di Leonardo, F. Ianni, G. Ruocco, Colloidal attraction induced by a temperature gradient, Langmuir 25 (2009) 4247.
[15] D.A. Belousov, V.S. Terent'ev, E.V. Spesivtsev, and V.P. Korolkov, Spectral data of refractive index and extinction coefficient for thin films of titanium group metals used for fabrication of optical microstructures. *Data Br.* **28**, 1 (2020).
[16] E. Flores-Flores, S.A. Torres-Hurtado, R. Páez, U. Ruiz, G. Beltrán-Pérez, S.L. Neale, J.C. Ramirez-San-Juan, R. Ramos-García, Trapping and manipulation of microparticles using laser-induced convection currents and photophoresis, Biomed. Opt. Express 6 (2015) 4079.
[17] J.A. Zenteno-Hernandez, J. Vazquez-Lozano, J.A. Sarabia-Alonso, J. Ramirez-Ramirez, R. Ramos-Garcia, Optical trapping in the presence of laser-induced thermal effects, Opt. Lett. 45 (2020) 1.
[18] J.A. Sarabia-Alonso, J.G. Ortega-Mendoza, J.C. Ramírez-San-Juan, P. Zaca-Morán, J. Ramírez-Ramírez, A. Padilla-Vivanco, F.M. Muñoz-Pérez, R. Ramos-García, Optothermal generation, trapping, and manipulation of microbubbles, Opt. Express 28 (2020).
[19] L.Q. Costa Campos, C.C. De Souza Silva, S.W.S. Apolinario, Structural phases of colloids interacting via a flat-well potential, Phys. Rev. E - Stat. Nonlinear, Soft Matter Phys. 86 (2012) 1.
[20] C.R. Nugent, K.V. Edmond, H.N. Patel, E.R. Weeks, Colloidal glass transition observed in confinement, Phys. Rev. Lett. 99 (2007) 1.
[21] E. Papp, G. Vigh, Role of buffer cations in the reversed-phase high-performance liquid chromatography of aromatic amines. I. methanol-rich eluents, J. Chromatogr. A 259 (1983) 49.
[22] R.J.M. Vervoort, F.A. Maris, H. Hindriks, Comparison of high-performance liquid chromatographic methods for the analysis of basic drugs, J. Chromatogr. A 623 (1992) 207.
[23] W. Wang, B. Gu, L. Liang, W.A. Hamilton, Fabrication of near-infrared photonic crystals using highly-monodispersed submicrometer SiO2 spheres, J. Phys. Chem. B 107 (2003) 12113.

[24] F. Piret, B.L. Su, Effects of pH and ionic strength on the self-assembly of silica colloids to opaline photonic structures, Chem. Phys. Lett. 457 (2008) 376.
[25] S. Ferraris, M. Cazzola, V. Peretti, B. Stella, S. Spriano, Zeta potential measurements on solid surfaces for in Vitro biomaterials testing: surface charge, reactivity upon contact with fluids and protein absorption, Front. Bioeng. Biotechnol. 6 (2018) 1.
[26] M. Kosmulski, The significance of the difference in the point of zero charge between rutile and anatase, Adv. Colloid Interface Sci. 99 (2002) 255.
[27] G. Trefalt, M. Borkovec, Overview of DLVO theory, Lab. Colloid Surf. Chem. Univ. Geneva 1 (2014).
[28] F. Giorgi, D. Coglitore, J.M. Curran, D. Gilliland, P. Macko, M. Whelan, A. Worth, E.A. Patterson, The influence of inter-particle forces on diffusion at the nanoscale, Sci. Rep. 9 (2019) 1–6.
[29] A. Yethiraj, Tunable colloids: control of colloidal phase transitions with tunable interactions, Soft Matter 3 (2007) 1099.
[30] J.C. Everts, M. Ravnik, Complex electric double layers in charged topological colloids, Sci. Rep. 8 (2018) 1.
[31] J. Kim, D.F. Lawler, Characteristics of zeta potential distribution in silica particles, Bull. Korean Chem. Soc. 26 (2005) 1083.
[32] R. Kesavamoorthy, S. Tandon, S. Xu, S. Jagannathan, S.A. Asher, Self-assembly and ordering of electrostatically stabilized silica suspensions, J. Colloid Interface Sci. 153 (1992) 188.